PILOT FOR AUTOMATED DETECTION AND CLASSIFICATION OF ROAD SURFACE DEGRADATION FEATURES

November 2003

JHR 03-293 Project 02-11

Bahram Javidi
Jack Stephens
Sherif Kishk
Thomas Naughton
John McDonald
Atef Isaac

This research was sponsored by the Joint Highway Research Advisory Council (JHRAC) of the University of Connecticut and the Connecticut Department of Transportation and was carried out through the Connecticut Transportation Institute at the University of Connecticut.

Technical Report Documentation Page

1. Report No.	2. Government Accession No.	3. Recipient's Catalog No.
JHR 03-293	N/A	N/A

4. Title and Subtitle	5. Report Date
PILOT FOR AUTOMATED DETECTION AND CLASSIFICATION OF ROAD SURFACE DEGRADATION FEATURES	November 2003
	6. Performing Organization Code: N/A

7. Author(s)	8. Performing Organization Report No.
Bahram Javidi, Jack Stephens, Sherif Kishk, Thomas Naughton, John McDonald, Atef Isaac	JHR 03-293

9. Performing Organization Name and Address	10. Work Unit No. (TRAIS)
University of Connecticut Connecticut Transportation Institute Storrs, CT 06269-5202	N/A
	11. Contract or Grant No.: N/A

12. Sponsoring Agency Name and Address	13. Type of Report and Period Covered
Connecticut Department of Transportation 280 West Street Rocky Hill, CT 06067-0207	FINAL
	14. Sponsoring Agency Code: N/A

15. Supplementary Notes

N/A

16. Abstract

This report deals with the detection and classification of pavement cracks. Currently, ConnDOT is using Wisecrax® which is a commercial product supplied by Roadware. However, Wisecrax® has some shortcomings. We proposed seemingly different techniques based on wavelet and Hough transforms; since the problem at hand must be analyzed in both the spatial and frequency domains. Two main algorithms had been developed for elimination of false detection, and for more accurate detection. The proposed techniques require less user intervention, and showed promising results. Some road images had been analyzed, specifically those which Wisecrax® did not analyze well. Since we tested our algorithms against highly compressed road images, some parts of the cracks were not detected, causing errors in crack length measurements.

17. Key Words	18. Distribution Statement
Crack Detection, Pavement Distress, Pattern Classification	No restrictions. This document is available to the public through the National Technical Information Service Springfield, Virginia 22161

19. Security Classif. (of this report)	20. Security Classif. (of this page)	21. No. of Pages	22. Price
Unclassified	Unclassified	40	N/A

Form DOT F 1700.7 (8-72) Reproduction of completed page authorized

ACKNOWLEDGEMENTS

The authors are grateful for all the members of
the Division of Pavement Management and Data Services
of the Connecticut Department of Transportation,
In Newington and Rocky Hill
for their help and support.

SI* (MODERN METRIC) CONVERSION FACTORS

APPROXIMATE CONVERSIONS TO SI UNITS

Symbol	When You Know	Multiply By	To Find	Symbol
		LENGTH		
in	inches	25.4	millimetres	mm
ft	feet	0.305	metres	m
yd	yards	0.914	metres	m
mi	miles	1.61	kilometres	km
		AREA		
in^2	square inches	645.2	millimetres squared	mm^2
ft^2	square feet	0.093	metres squared	m^2
yd^2	square yards	0.836	metres squared	m^2
ac	acres	0.405	hectares	ha
mi^2	square miles	2.59	kilometres squared	km^2
		VOLUME		
fl oz	fluid ounces	29.57	mililitres	mL
gal	gallons	3.785	Litres	L
ft^3	cubic feet	0.028	metres cubed	m^3
yd^3	cubic yards	0.765	metres cubed	m^3

NOTE: Volumes greater than 1000 L shall be shown in m^3

		MASS		
oz	ounces	28.35	grams	g
lb	pounds	0.454	kilograms	kg
T	short tons (2000 lb)	0.907	megagrams	Mg
		TEMPERATURE (exact)		
°F	Fahrenheit temperature	5(F-32)/9	Celcius temperature	°C

* SI is the symbol for the International System of Measurement

APPROXIMATE CONVERSIONS TO SI UNITS

Symbol	When You Know	Multiply By	To Find	Symbol
		LENGTH		
mm	millimetres	0.039	inches	in
m	metres	3.28	feet	ft
m	metres	1.09	yards	yd
km	kilometres	0.621	miles	mi
		AREA		
mm^2	millimetres squared	0.0016	square inches	in^2
m^2	metres squared	10.764	square feet	ft^2
ha	hectares	2.47	acres	ac
km^2	kilometres squared	0.386	square miles	mi^2
		VOLUME		
mL	millilitres	0.034	fluid ounces	fl oz
L	litres	0.264	gallons	gal
m^3	metres cubed	35.315	cubic feet	ft^3
m^3	metres cubed	1.308	cubic yards	yd^3
		MASS		
g	grams	0.035	ounces	oz
kg	kilograms	2.205	pounds	lb
Mg	megagrams	1.102	short tons (2000 lb)	T
		TEMPERATURE (exact)		
°C	Celcius temperature	1.8C+32	Fahrenheit temperature	°F

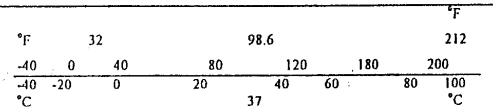

TABLE OF CONTENTS

LIST OF FIGURES

LIST OF TABLES

SYMBOLS

$\theta(x, y)$: Cubic spline function.

$\psi^1(x, y)$: Quadratic spline mother wavelet function, the derivative of $\theta(x, y)$ with respect to the x direction.

$\psi^2(x, y)$: Quadratic spline mother wavelet function, the derivative of $\theta(x, y)$ with respect to the y direction.

$\psi_S{}^1(x, y)$: Dilation of the mother wavelet $\psi^1(x, y)$ by a scaling factor *s*.

$\psi_S{}^2(x, y)$: Dilation of the mother wavelet $\psi^2(x, y)$ by a scaling factor *s*.

$W^1 f(s, x, y)$: Wavelet transform of $f(x, y)$, with respect to the x direction.

$W^2 f(s, x, y)$: Wavelet transform of $f(x, y)$, with respect to the y direction.

$Mf(s, x, y)$: Magnitude of the wavelet transform of $f(x, y)$ at scale *s*.

$Af(s, x, y)$: Angle of the wavelet transform of $f(x, y)$ at scale *s*, measured with respect to the x direction.

(r, θ): coordinates of point (x,y) in the spatial domain, projected in the Hough transform domain.

1. The Wisecrax® integrated software

Wisecrax® provides a comprehensive suite of tools for the automated detection and classification of pavement distress in photolog images. These images are collected by the ARAN vehicle using two downward facing, rear-mounted cameras. To ensure that each frame records a different section of road, the frame rates of the cameras are varied dynamically based on the vehicles speed. High-powered strobe lights are used to eliminate shadows due to overhead power-lines, trees, etc. The video streams from both cameras are interleaved and recorded onto an S-VHS tape for offline processing. The images were interweaved during the acquire step of the processing in the office. The Wisecrax® workstation demultiplexes these two streams and combines them to provide a single continuous image of the lane. Each camera creates a 1.5 by 2 meters images, which can be combined to construct the whole image of the curb. Each continuous image can be 10 meters, 20 meters, or $1/100^{th}$ of a mile each with a width of approximately 4 meters. When detecting cracks, Wisecrax® can operate in a number of modes. The most important of these is batch mode where Wisecrax® processes a large (up to 40km) portion of road without human intervention. Human intervention is needed in the initial setting and quality control checking. The output of Wisecrax® is a crack map for each section of road and statistics summarizing the pavement condition.

The S-VHS Tape has been replaced with digital cameras to enhance the quality of the images and eliminate old VHS recorder/players equipment and associated multi connections, which reduced the image quality with each connection since the initial research was conducted.

2. Description of progress

Since the beginning of the project a number of meetings have been held with the ConnDOT Pavement Management Division and Research and Materials Division. Details of the meetings held are listed below:

11 July – (Half-day) Met with members of the Connecticut Advanced Pavement Laboratory to discuss the forms of pavement distress and its causes.

12 July – (Full-day) Meetings with ConnDOT Pavement Management and Materials and Research Divisions. Introduced to the Photo-log data collection process and, the Wisecrax® automated pavement distress analysis system.

17 July – (Half-day) Meeting to collect and review photo-log data from ConnDOT Pavement Management.

25 July – (Full-day) Familiarization and data processing with the Wisecrax® computer system.

13 August – (Full-day) Data processing with the Wisecrax® computer system.

The meetings focused on the familiarization with the pavement data collection process and the Wisecrax® automated pavement distress analysis system used by ConnDOT. Capabilities of the system were assessed in terms of crack detection and width estimation. Personnel of the Division of Pavement Management provided input on the aspects of the Wisecrax® system that needs improvement.

3. Determination of Wisecrax shortcomings

From discussions with ConnDOT pavement management personnel, the following problems were identified as key weaknesses in the system.

1. High level of quality control required

The Wisecrax® system operator must determine the parameter values for detection and carry out quality control checks. Daily control check involves reviewing the image with the crack superimposed in order to verify accuracy of the pavement surface characteristics produced. Depending on the pavement surface characteristics, this quality control may need to be applied exhaustively over an entire batch. Due to its expensive nature ConnDOT would like to reduce this requirement.

2. Setting of parameters for processing

Prior to processing each batch of images the operator must set five system parameters through a trial-and-error process to achieve the desired level of detection.

3. False cracks appearing due to white paint

Prior to crack detection, Wisecrax® appears to apply an adaptive contrast enhancement procedure to the images. This results in the introduction of dark bars along the edge of white road delineations. These dark bars cause the detection of a high number of false cracks. Any transverse pavement markings, manholes and other items are duplicated during the normalization process. The replicated cracking patterns of these items are identified as false cracking and are eliminated during the quality control process.

4. Saturation of Charge Coupled Devices (CCDs) due to retro-reflective glass beads on newly laid pavement

The high retro-reflectivity of the fresh paint markings causes the CCD sensors to become saturated. (The current CCD sensors have an 8-bit dynamic range).

5. Storage of the data on analog S-VHS prior to digitization and processing

Storage of the images in an intermediate analog format causes reduced image quality. Roadware Inc. has identified this problem and is now upgrading to completely digital systems. ConnDOT has upgraded the Wisecrax camera image system to a completely digital system since the initial research of this paper.

6. False crack detection

The Wisecrax® system is incapable of dealing with extraneous objects or features in the pavement images. The most common of these objects include: tire marks, paint, repaired road, stop lines, manhole covers, read bridge joints, and grates.

In some instances, when false cracks are detected the Wisecrax® algorithm mistakenly detects a false crack at the same lateral position periodically through the sequence.

7. Change in road conditions

Wet road surface results in high false crack detection hence data collection may only be carried out during dry weather conditions.

8. Formation of continuous image is imprecise

In forming a continuous road image, Wisecrax® digitizes the frames from the S-VHS and combines them into a continuous image. Part of this process requires aligning the image streams. The Wisecrax® system is not robust and causes both cropping and repetition of image data along the center of the lane.

4. Clutter removal

When a section of a road is processed by the Wisecrax® system the outputs occasionally contain a large number of false detections due to change in the pavement texture, foreign objects such as manhole covers, transverse line stripping (stop bar, walkways), railroad tracks, and traffic loops. It is the system operator's task to manually remove these false cracks during the QA (quality assurance) stage. This process is laborious. It was decided with ConnDOT Pavement Management that the algorithms developed in this project would concentrate on reducing this subjectivity.

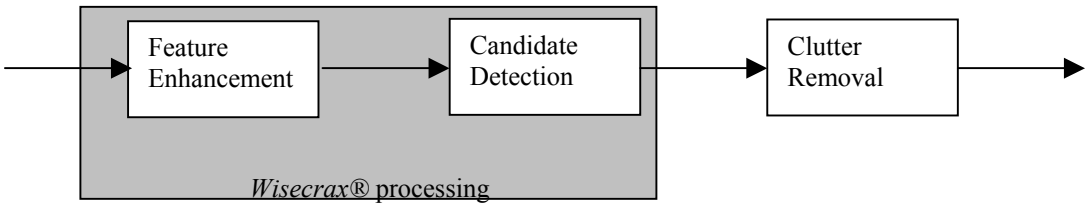

Figure 1. Enhancement to the Wisecrax® system.

Since the source code and algorithms employed by the Wisecrax® system are not released by Roadware, the system has to be viewed as a *black box*. That is, the only assumption made about the system is that it is capable of outputting the locations of the cracks, where this output is (possibly) contaminated with a large number of false detections. In this project we will develop post-processing techniques, as shown in Figure 1, to perform clutter removal on this data, i.e. to remove the false cracking (see Figures 2-4).

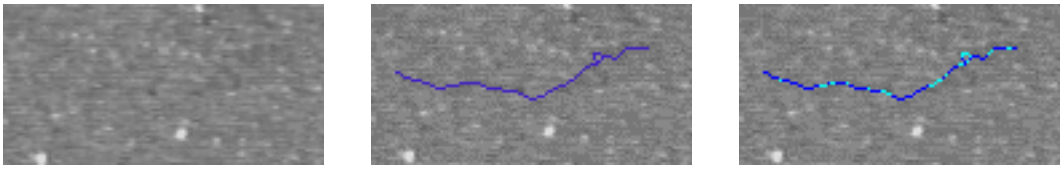

(a) (b) (c)

Figure 2. (Sec. 273016235): (a) Original Image; (b) False Detection of a crack by Wisecrax®; (c) False Detection Revealed as multicolored cracks

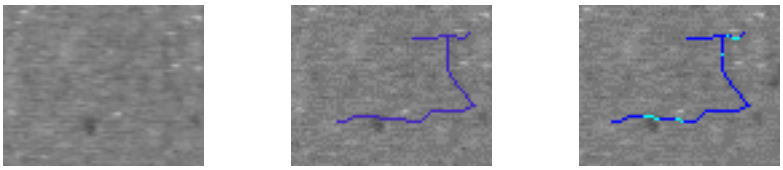

(a) (b) (c)

Figure 3. (Sec. 273016235): (a) Original Image; (b) False Detection of a crack by Wisecrax®; (c) False Detection Revealed as multicolored cracks.

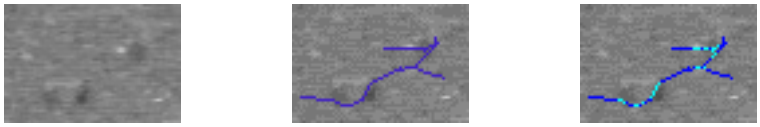

(a) (b) (c)

Figure 4. (Sec. 273016235): (a) Original Image; (b) False Detection of a crack by Wisecrax®; (c) False Detection Revealed as multicolored cracks.

The advantage of this approach is that rather than applying a computationally complex technique to the entire image, a simple technique (the Wisecrax® technique) is used for detecting candidate cracks and hence reducing the search space. Next, a more sophisticated and typically computationally complex technique (our enhancement) can be applied without a significant increase, portion of a second per image, in running time, since it is only applied to the candidate regions identified in the previous stage. This decoupling yields a more computationally acceptable approach, and allows more independent control of system's false accept and false reject rates. It also has the added advantage of integrating the previous computing and software infrastructure into current developments.

As mentioned above, as part of the meetings with ConnDOT personnel a thorough introduction was provided to the Wisecrax® computer system and the methods of data collection used in ConnDOT. During July and August 2002 a number of day-long visits were made to ConnDOT to become familiar with the Wisecrax® system. The objective of these visits was to get hands-on experience with the system's capabilities and to generate data to be used for *System Development* and *Future Research Planning*.

5. Literature review

An extensive review of the literature was performed to determine the approaches applied to date. Automated pavement distress analysis through image processing techniques has been the subject of research since the late 1980's. Initial attempts to solve the problem centered on histogram and edge based techniques. However, due to the highly textured nature of road surface images, the lack of spatial coherence in image intensity causes such techniques to fail. In an attempt to overcome these problems a number of statistical approaches were applied to the problem. Modern approaches using a combination of these techniques in conjunction

with matched filtering have been shown successful under limited conditions. One of the problems encountered in reviewing the approaches is the lack of objective and repeatable performance evaluation.
In parallel with this survey, state-of-the-art theories of texture segmentation and a wavelet based techniques were investigated and assessed in terms of their applicability to the problem.

6. Problems encountered

Road images we managed to get from the output of the Wisecrax® system are highly compressed JPEG images, which wipes out a lot of the fine details of the higher resolution original images in the video sequence, also due to the artifacts introduced by block dividing of the JPEG algorithm, a lot of artificial block edges have been introduced in the compressed images. Another problem we faced while processing JPEG images is the spatial enlargement of high frequency texture in the asphalt caused by the suppression of high frequency components of the discrete cosine transform, which mislead our detection algorithm, causing false cracks detections.

7. System development

Initial investigations were performed with the collected data. Tools have been developed to allow researchers at UConn to access the relevant crack information and to align this information with the associated image pixels.

A clutter-removal technique had been developed, This technique computes a collection of image features across the candidate crack. To do this, the orientation of the crack is computed at each point. Pixels positioned orthogonal to the crack and within a specified range are extracted. These pixel values are used in computing features at this point. Each feature becomes an element of a feature vector associated with that point. This vector of values is computed at a set of discrete intervals along the crack. Using this set of vectors a decision is made on whether or not the candidate should be removed. Results are shown in Figures. 2, 3, 4.

For cracks detection and classification, a technique, based on Wavelet Multi-scale edge detection, has been developed and tested with sections of the road with a variety of cracks shapes; most of which Wisecrax® failed to detect. This technique is the most robust at hand, and proves to be very effective for high resolution images. It is based on edge detection on different wavelet decomposition scales, which enables tracking of true cracks, and excluding false detections caused by noisy texture in the image asphalt background.

However, this technique is not totally exploited because the road images we have at hand are JPEG compressed. JPEG compression, images are first partitioned into 8x8 blocks that are independently transformed using block Discrete Cosine Transform (DCT), then quantized and entropy coded. JPEG introduces blocking artifacts at medium and high compressions because of its short and non-overlapping

basis Discrete Cosine function. JPEG also suffers from ringing artifacts at high compression. Both artifacts are clearly visible at the images we obtained as an output from Wisecrax®. We must extract the road images directly from the original video recordings ConnDOT has. Original images are high-resolution images, and strongly believed to reveal excellent and accurate crack detection results. The ConnDOT team is working to upgrade the system to eliminate the numerous locations where the image quality could be affected. The images we have at hand are highly compressed (DCT-based JPEGs) versions just displayed for user convenience and storage purposes by Wisecrax®, typically the JPEGs we have are believed to be compressed with a ratio of 1:5. This compression wipes out important details that can help fine-tuning the crack detection process. This compression is responsible for the false detection of background noise as cracks, as will be shown in our results.

The proposed technique does not require a great deal of user intervention as Wisecrax®. In Wisecrax®, the operator is required to judge the presence of true cracks by his eyes for each road section, and adjust different parameters. Our proposed technique is robust to variations in brightness and contrast of different images; since it relies on comparisons of wavelet coefficients obtained from different wavelet decompositions levels of the same individual image. Also, it includes pixels as parts of a crack based on local measures in the neighborhood of that pixel, not on measures extracted from the whole road section image.

Conventional edge detection techniques (Canny, Sobel, …) fails to detect correct edges due to the inherent noise in the road images, added to that are the low resolution and quantization noise introduced by loss compression of those images, which are also detected as edges; because of the sharp intensity variation it introduces. Please review section 11.1, where it is shown our crack detection results compared to Canny edge detection.

Before discussing the wavelet based techniques used, we would like to point out some important differences between Fourier analysis and wavelets decompositions. Fourier basis functions are localized in frequency but not in spatial domain. Small frequency changes in the Fourier transform will produce changes everywhere in the whole spatial domain, and it will fail to detect and discriminate important edges (spatially long cracks) from other spatially small background noise on the road section. On the other hand, wavelets are local in both frequency/scale (via dilations) and in spatial domain (via translations). This localization is advantageous in many cases, like crack detection because cracks extends for long distances in the spatial domain (spatially long), and this is what signifies cracks from other random background noise scattered all over the noisy image. Also, wavelet-based algorithms are invariant to non-uniform illumination, shadows, and scaling distortions, which will be deteriorating factors in our detection procedure.

It has been proved that the wavelet transform is closely related to multi-scale edge detection, because the local maxima of a wavelet transform are equivalent to detecting the location of irregular structures using edge detectors (Canny as an

example). Important edges and noise are two types of singularities in the intensity image. The wavelet transform has different behaviors for both singularities because noise contains faster oscillations than important edges. We will show how to discriminate important edges from noises by analyzing the behavior of the wavelet transform local maxima through multiple decompositions on different scales. It is well known that the edge points at a certain scale are the points where the modulus of the wavelet transform gradient vector is maximum in the direction where this gradient vector points too. We use the same approach to define the local maxima of the wavelet transform, where the scale s varies only along increasing discrete values of the dyadic sequence 2^j.

8. Principles of 2-D image wavelet transform

We define two wavelets which are respectively the partial derivatives along x and y of a two-dimensional smoothing cubic spline wavelet function $\theta(x,y)$.

$$\psi^1(x,y)=\frac{\partial\theta(x,y)}{\partial x} \quad \text{and} \quad \psi^2(x,y)=\frac{\partial\theta(x,y)}{\partial y}$$

Let $\psi_S{}^1(x,y)=\left(\frac{1}{s}\right)^2\psi^1\left(\frac{x}{s},\frac{y}{s}\right)$ and $\psi_S{}^2(x,y)=\left(\frac{1}{s}\right)^2\psi^2\left(\frac{x}{s},\frac{y}{s}\right)$, Where the subscript s denotes dilation by a scaling factor.

For any 2-D image, where $f(x,y)$ is the intensity at pixel (x,y), the wavelet transform defined with respect to $\psi^1(x,y)$ and $\psi^2(x,y)$ has two components:

$W^1f(s,x,y)=f*\psi_S{}^1(x,y)$ and $W^2f(s,x,y)=f*\psi_S{}^2(x,y)$.

where $*$ is the convolution operator.

$$\begin{pmatrix}W^1f(s,x,y)\\W^2f(s,x,y)\end{pmatrix}=s\begin{pmatrix}\frac{\partial}{\partial x}(f*\theta_s)(x,y)\\\frac{\partial}{\partial y}(f*\theta_s)(x,y)\end{pmatrix}=s\vec{\nabla}(f*\theta_s)(x,y)$$

Defining $Mf(2^j,x,y)=\sqrt{\left|W^1f(2^j,x,y)\right|^2+\left|W^2f(2^j,x,y)\right|^2}$ as the modulus of the wavelet transform at scale 2^j.

Hence, the two components of the wavelet transform are the coordinates of the gradient vector of $f(x,y)$ smoothed by $\theta_s(x,y)$. Canny defines the edge points of $f(x,y)$ at the scale s as the points where the modulus of the gradient vector of $f(x,y)*\theta_s(x,y)$ is maximum in the direction where the gradient vector points too, it is the direction where $f(x,y)$ has the sharpest variation.

At each scale 2^j , the local maxima of the wavelet transform are the points (x, y) where the modulus image $Mf(2^j, x, y)$ is locally maximum along the gradient direction given by $Af(2^j, x, y) = \tan^{-1}\left(\frac{W^2 f(2^j, x, y)}{W^1 f(2^j, x, y)}\right)$. The local maxima are inflection points of $f(x, y) * \theta_{2^j}(x, y)$. We record the position of each of these local maxima and the values of $Mf(2^j, x, y)$ and $Af(2^j, x, y)$ at the corresponding location at scale 2^j. An interesting class of image irregularities is the one where locally the function $f(x, y)$ is singular in one direction but varies smoothly in the perpendicular direction. Those irregularities might have nearly the same constant local maxima amplitude that belongs to a smooth curve in the image plane $f(x, y)$. These curves are the important cracks in the image structures. We thus reorganize the maxima representation into chains of local maxima to recover these crack curves. To chain a crack point with its neighbors, we use the fact that the orientation of the gradient angle given by $Af(2j,x,y)$, is perpendicular to the tangent of the crack curve that goes through this point.

We can separate background noise from the important Cracks by measuring the evolution across scales of the wavelet transform maxima. Also, knowledge of the geometrical properties of the important edges can also be used to chain modulus maxima which belong to smooth maxima crack curves. We chain two adjacent local maxima if their respective position is perpendicular to the direction indicated by $Af(2^j, x, y)$, and the modulus $Mf(2^j, x, y)$ have close values. On the contrary, the sharp variation points of background noise do not create such smooth curves of $Mf(2^j, x, y)$, and $Af(2^j, x, y)$, so they will not be chained, and will not be a part of our crack map. We also remove all the chains whose length is smaller than a given threshold, and all the maxima that do not propagate up to the scale 2^3 or propagate with an average value that increases when the scale decreases. This means that this regularity is basically a part of background noise. This procedure suppresses most of the maxima created by the background noise.

Due to the noisy nature of the road sections images, parts of the cracks are completely wiped out, forming gaps in the detected cracks, and can only be recovered by judging its location, orientation, and intensity with respect to location, orientation, and intensity of the detected cracks. This problem can be overcome by projecting our crack map images into the Hough transform domain, which can be used as a handy tool for quantifying the number of dominant cracks in a given image, and will help us in testing the gaps that should be included as parts of the cracks map.

9. Principles of Hough transform

In recent years the Hough transform has received much attention. This transform is able to transform two-dimensional images with lines into a domain of possible line parameters, where each line in the image will give a peak positioned at the corresponding line parameters. This has led to many line detection applications

within image processing, computer vision, and seismic. Figure 5 illustrates the principle of Hough transform.

- The main advantage of the Hough transform is that it is tolerant of gaps in feature boundary descriptions and is relatively unaffected by image noise.
- The Hough transform is a technique which can also be used to isolate features of a particular shape within an image, and can be employed in applications where a simple analytic description of a feature(s) is not possible.
- The Hough transform can be used to extract feature boundaries which can be described by regular curves or straight lines, and it is useful for computing a global description of features (where the number of solution classes need not be known *a priori*), given (possibly noisy) local measurements.
- The motivating idea behind the Hough transform technique for line detection is that each input measurement (*e.g.* coordinate point) indicates its contribution to a globally consistent solution (*e.g.* the physical line which gave rise to that image point).

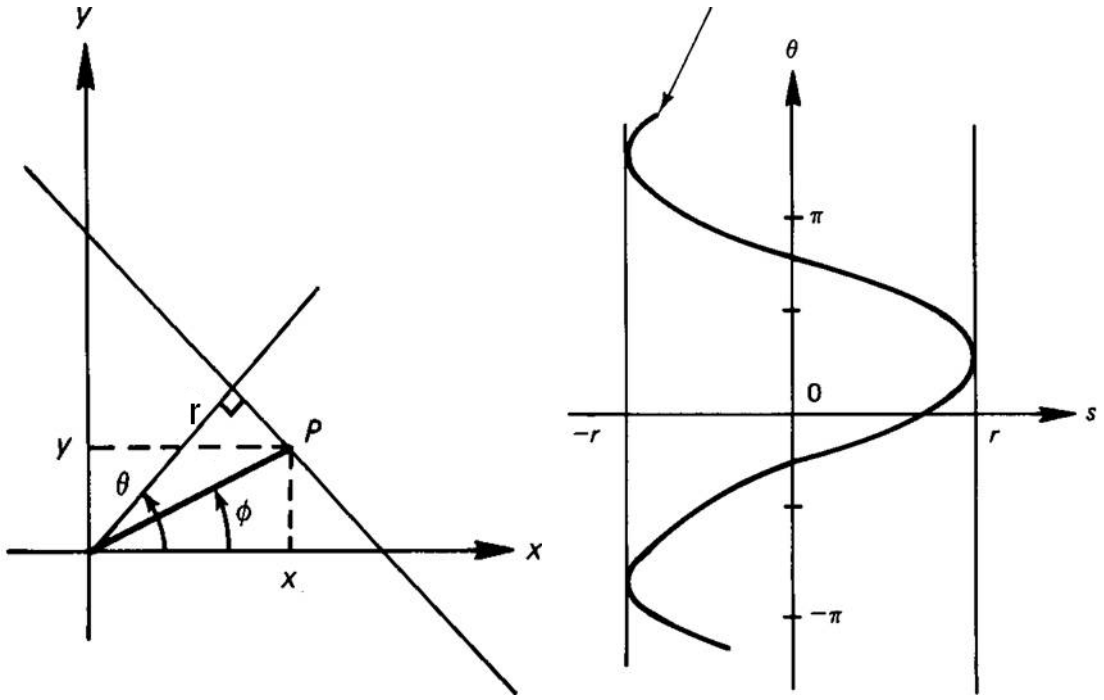

(a) (b)

Figure 5. The Hough Transform (a) A line in the spatial domain; (b) Locus of a point ρ in the projection plane (Hough transform).

In an image analysis context, the coordinates of the point(s) of edge segments (*i.e.* (x, y)) in the image are known and therefore serve as constants in the parametric

line equation, while r and θ are the unknown variables we seek. If we plot the possible r and θ values defined for each (x, y), points in image spatial domain map to curves (*i.e.* sinusoids) in the polar Hough parameter space. This *point-to-curve* transformation is the Hough transformation for straight lines. When viewed in Hough parameter space, points which are collinear in the cartesian image space become readily apparent as they yield curves which intersect at a common point r_o and θ_o.

The transform is implemented by quantizing the Hough parameter space into finite intervals or *accumulator cells*. (i.e. a multidimensional array). As the algorithm runs, each (x, y) is transformed into a discretized (r, θ) curve and the accumulator cells which lie along this curve is incremented. Peaks in the accumulator array represent a strong evidence that a corresponding edge exists in the image. As cracks generally exist as two edges running side by side in an image, we expect an ideal crack to be revealed as two peaks at the same $\theta - coordinate$ (having the same orientation), and nearly of the same height (Crack length), and displaced by *d* in the r coordinate, which is the crack width in image pixels. Fig. 6.e shows three main peaks corresponding to the cracks detected in Fig. 6.a. After determining the orientation and displacement of each crack from the projection in the Hough transform domain, the cracked areas can be emphasized in another iteration and wavelet decompositions can be used again individually on each of those regions, to have more accurate detection of the cracks.

As experiments will show the Hough transform is a powerful tool for classifying cracks, it provides an estimate of the number of the cracks in the image, each individual crack length, and possibly its width.

10. Crack characteristics

10.1 Crack orientation

Orientation at every candidate crack pixel can be calculated as the angle of axis of the least moment of inertia of the crack part in a sliding window W of 7*7 pixels, so it is obtained by minimizing the moment of inertia $I(\theta_r)$ with respect to θ, where:

$$I(\theta_r) = \sum_{(m,n)\in W}\sum \left[(n-\bar{n})\cos\theta_r - (m-\bar{m})\sin\theta_r\right]^2; \qquad (\bar{m},\bar{n}) \text{ is the center of mass.}$$

So the orientation is given as:

$$\theta_{ro} = \frac{1}{2}\tan^{-1}\left[\frac{2\mu_{1,1}}{\mu_{2,0}-\mu_{0,2}}\right]$$

where $\mu_{p,q} = \sum_{(m,n)\in W}\sum (m-\bar{m})^p (n-\bar{n})^q$ is the (p,q) order central moment.

Crack orientation is chosen according to the orientation of most of its pixels, either longitudinal or transverse.

10.2. Crack width

After calculating crack pixels orientation, crack width at any pixel can be measured from the intensity variation perpendicular to the crack at that pixel within a window of 11 pixels wide, centered around that pixel. As the images we have are approximately 3100 pixels in height, and 990 pixels in width for each (Length = 10 *Width = 3) meters^2 section of the road; it can be assumed that the image resolution is 310 pixels/meter, or 0.31 pixels/mm.

10.3. Crack severity

Cracks are classified to 3 categories according to their severity level:

Low severity: Crack average width is greater than 0 mm, but less than 6 mm. In the crack map image this can be detected for crack average width less than 1.8 pixels.

Medium severity: Crack average width is greater than 6 mm, but less than 12 mm, which can be detected in the crack map image for crack average widths between 1.8 and 3.6 pixels.

High severity: Crack width is greater than 12 mm, which can be detected in the crack map image for crack average widths greater than 3.6 pixels.

However, we think that it is better to rely on crack widths at individual pixels as an indication of the severity of the crack, for example it is safer to consider the severity level as high if the crack width exceeds 4 pixels for a considerable length of the crack, even if the crack average width is still lower than 3.6 pixels.

10.4. Crack length

Actual crack length is proportional to the detected cracks in the image, with the same resolution calculated for measuring Crack width, 0.31 pixels/mm. However, due to the noisy asphalt background, some complicated crack structures (with segments having small radius of curvature) will be broken up into different sections. So, for cracks which are less than 30 cm. on the road, which is equivalent to 90 pixels in the images, we need to further investigate how those small sections can be joined with longer cracks. Integration around each peak in the Hough-transform domain gives a rough estimate of the length of that crack.
Crack length can be measured only once for the most obvious crack in the image (Highest peak in the Hough transform domain), other crack lengths need not be measured from the pixels traced in the image belonging to that crack. Instead, their peaks in the Hough transform domain are compared to the highest peak, and their lengths can be deduced accordingly by as a simple proportionality to the highest peak crack, i.e., we completely rely on the projected image (in the Hough transform domain) to measure cracks length for all but one of the cracks.

The following figures show the significance of the results obtained by applying wavelet multi-scale edge detection techniques coupled with using the Hough transform, compared to crack detection results obtained by Wisecrax®. Those are actual images obtained from ConnDOT of different sections of a BROOK Street in the state of Connecticut (27301600, BROO, 2640). It is evident that edge detection techniques based on wavelets decompositions provide more accurate results than Wisecrax®, although all images used are highly JPEG compressed. It is strongly believed that using the uncompressed images will provide much more accurate results.

11. Results

Section 273016000:

Figure 6-a shows a 512*512 pixels image, which is 1.7*1.7 meters^2 on the road. There are a lot of black and white spots scattered all over the image, which are detected as cracks by Canny's algorithm. However, most of those false cracks were excluded by our algorithm. As shown in Figure 6-c, Wisecrax® could detect a part of crack 3, but it completely failed to detect cracks 1 and 2. With no known reason, several other transverse cracks had been falsely detected. It can be seen that there are no true cracks other than the 3 visually apparent ones. Figure 6-d illustrates the cracks detected by multi-scale edge detection techniques. Figure 6-e. shows the 3 cracks in the Hough transform domain.

Crack 1 is located at $\theta = 168^\circ, r = -63$, θ is measured from the vertical axis, r is measured from point C, the center of the image, with positive sign if the perpendicular to the crack from C is above it, and negative otherwise. This is the sharpest (most concentrated) peak; since the crack is almost straight, and exhibits less winding than the 2 other cracks. The length of the crack is measured as described in section 10.4, and the average width is determined as described in to section 10.2.

Crack 2 is located at $\theta = 47^\circ, r = 19$. This is the least obvious crack, and it has the maximum dispersion around its peak. Crack 3 is shown to be at $\theta = 107^\circ, r = -36$. The length of the cracks is measured according to section 10.4, and the average width is determined according to section 10.2. Cracks classification and measurements results are shown in Table 1.

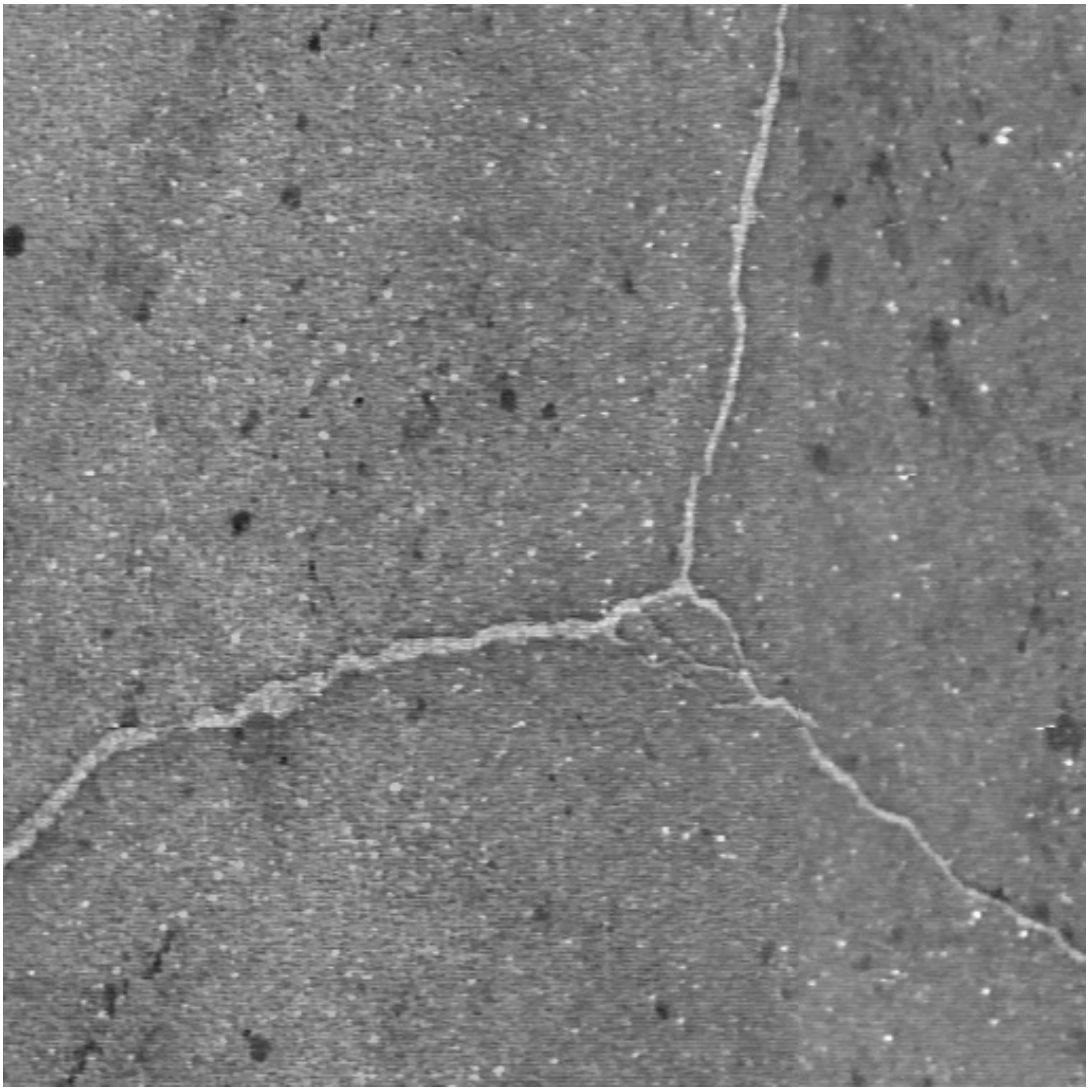

Figure 6-a. Original Image Sec. 273016000.

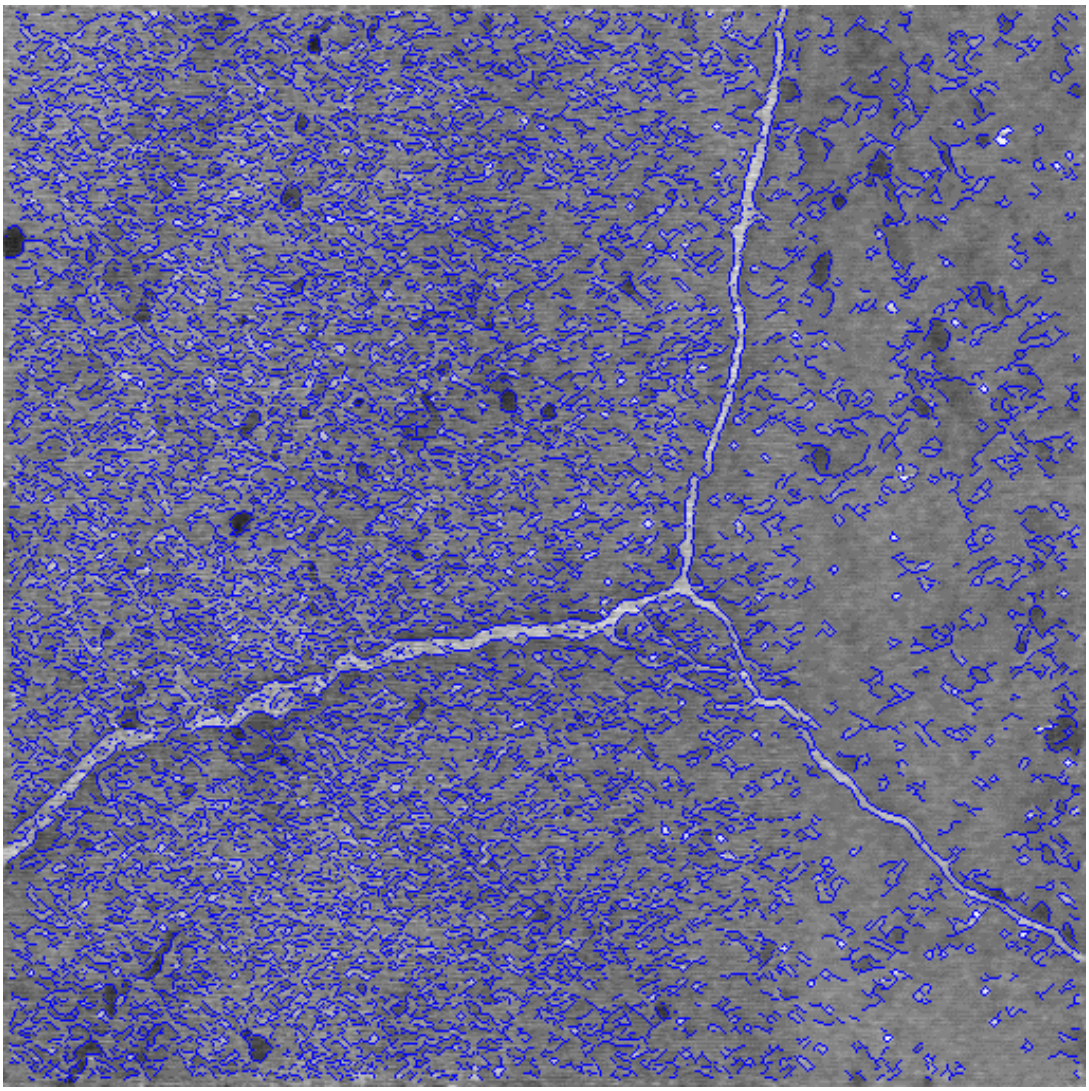

Figure 6-b. Cracks detected by Canny's edge detection algorithm.

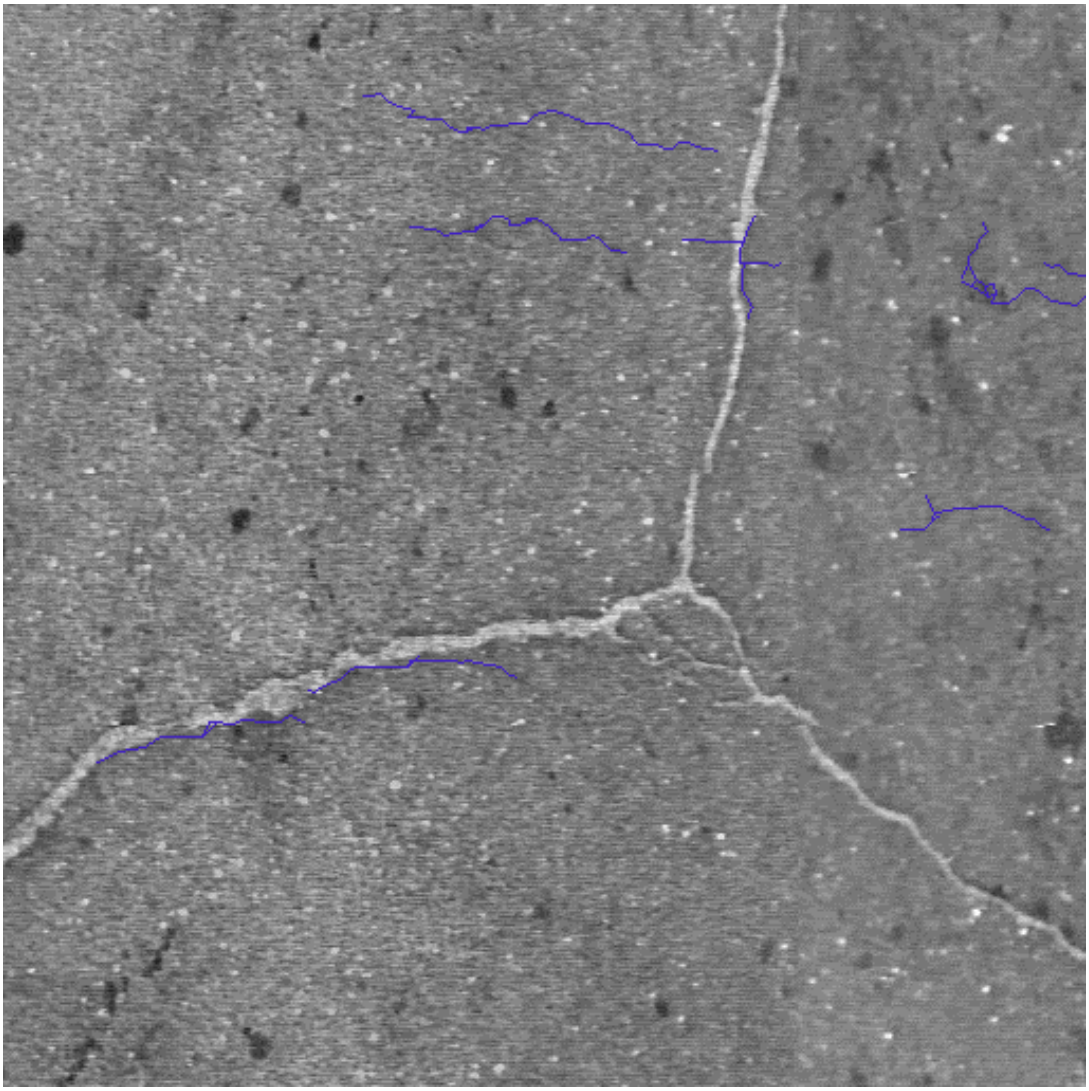

Figure 6-c. Cracks detected by Wisecrax®.

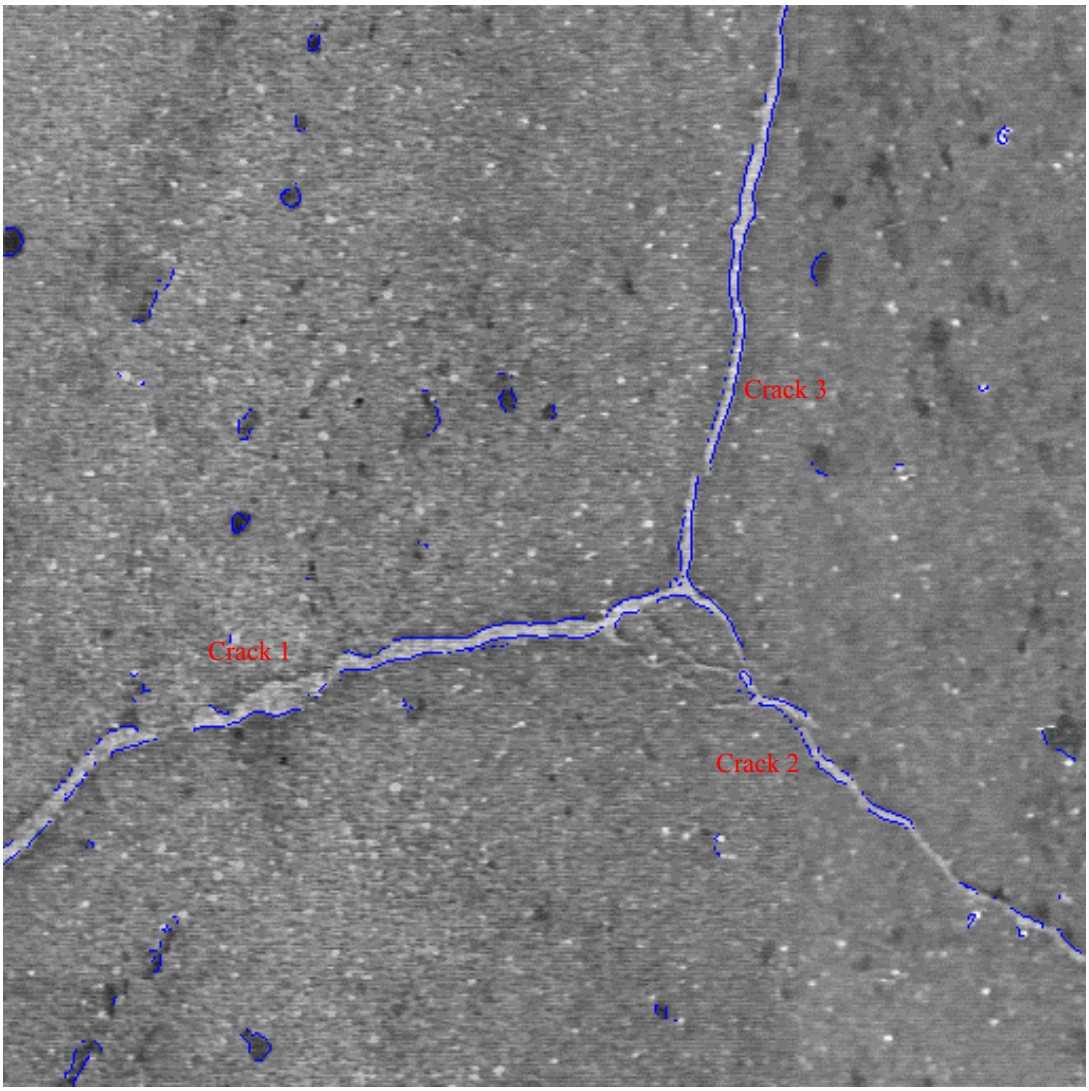

Figure 6-d. Cracks detected by multi-scale edge detection techniques.

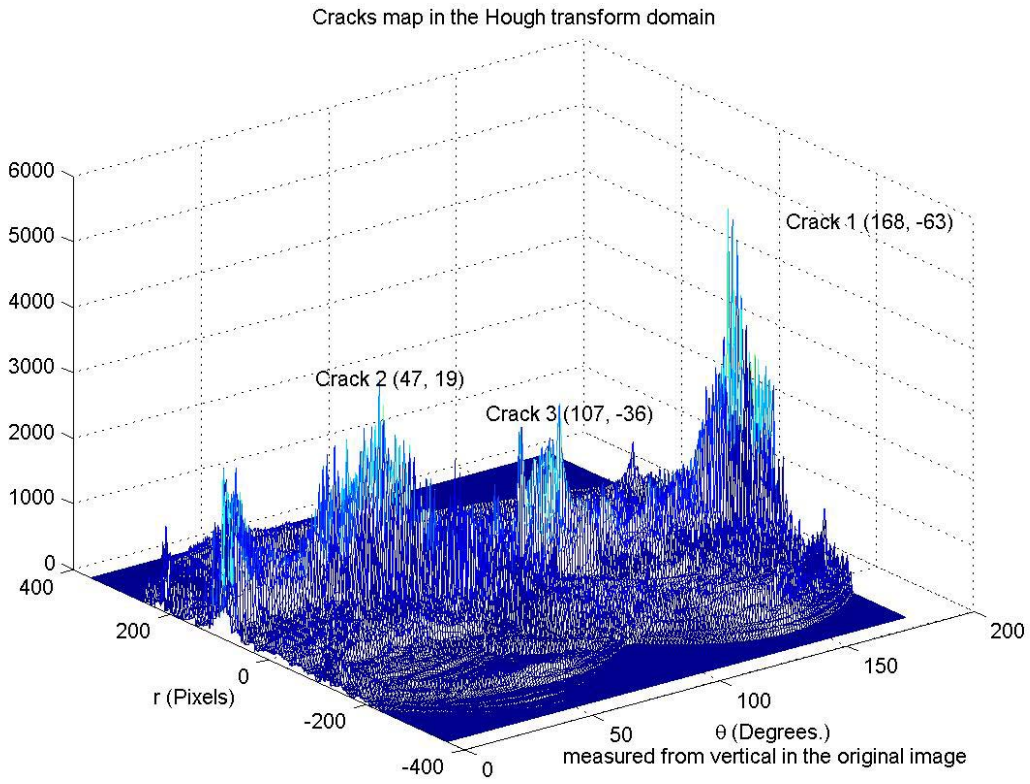

Figure 6-e. Cracks in the Hough transform domain. 3 main cracks are detected. θ measured from vertical in the original image.

Crack Number	Crack Length (m)	Crack Average Width (Pixels)	Crack Average Width (mm.)	Severity
1	0.73	3.91	13	High
2	0.38	3.85	12.8	High
3	0.67	3.94	13.3	High

Table 1. Results for Section 273016000

Section 27301600183:

Figure 7-a shows a 530*80 pixels image, which is 1.7*0.27 meters^2 on the road. This section is less noisy which enabled detecting most of the crack. Detection looks superior to Wisecrax®. There is one dominant transverse crack, which shows up at $\theta = 97^\circ, r = -2$. Cracks classification and measurements results are shown in Table 2.

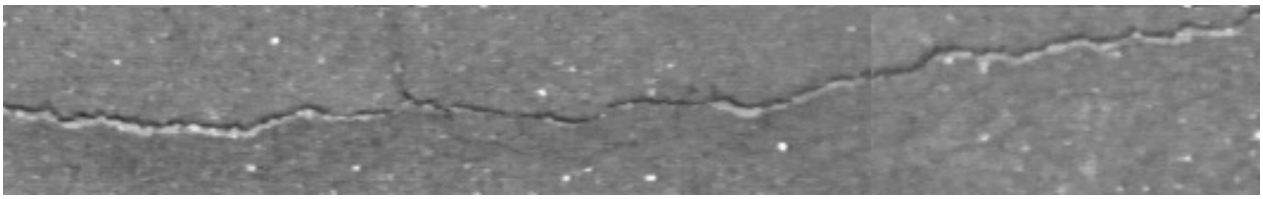

Figure 7-a. Original Image Sec. 27301600183

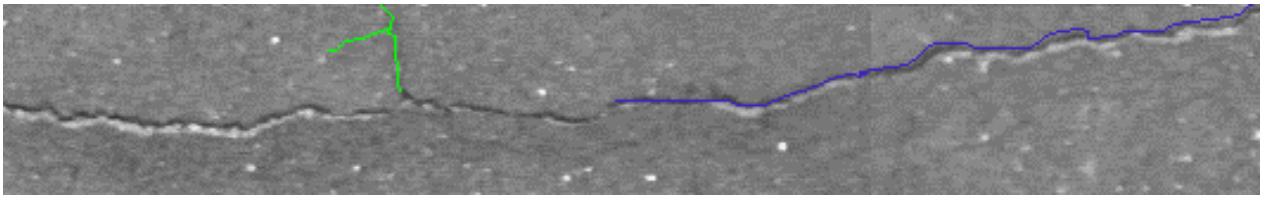

Figure 7-b. Cracks detected by Wisecrax®

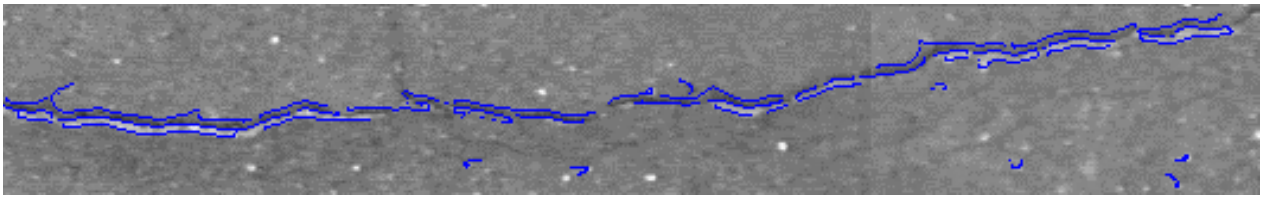

Figure 7-c. Cracks detected by multi-scale edge detection techniques.

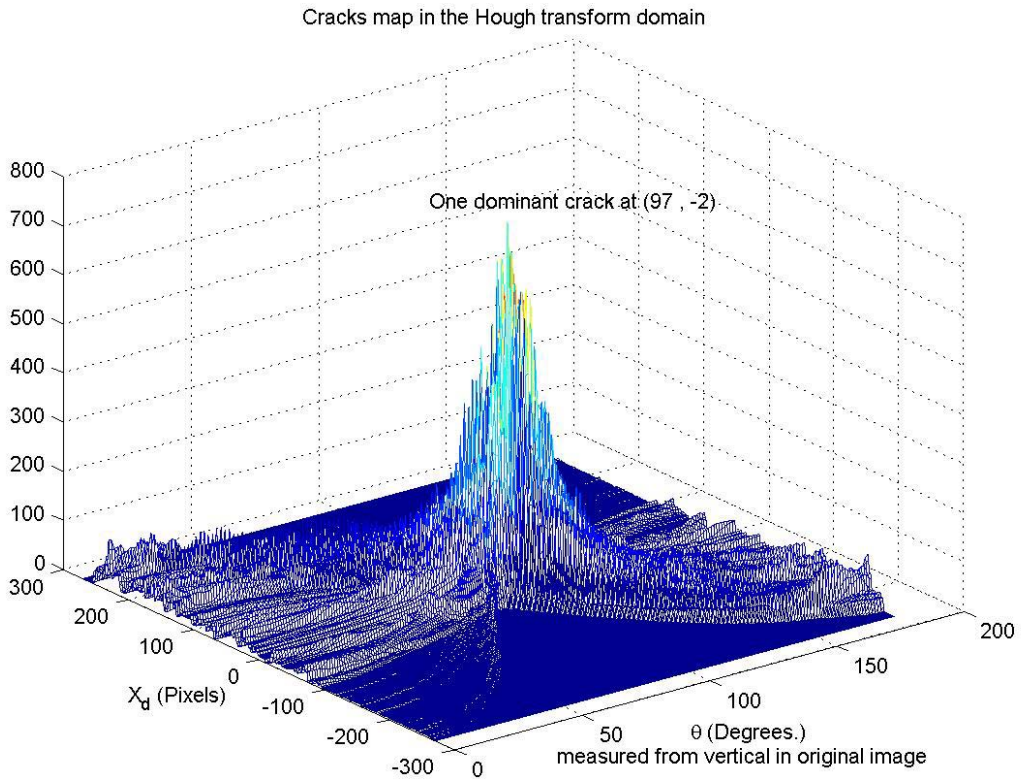

Figure 7-d. Cracks in the Hough transform domain. 1 crack is detected. θ measured from vertical in the original image.

Crack Number	Crack Length (m)	Crack Average Width (Pixels)	Crack Average Width (mm.)	Severity
1	1.63	4.51	15	High

Table 2. Results for Section 27301600183

Section 273016026:

Figure 8-a shows a 930*130 pixels image, which is 3*0.43 meters^2 on the road. It shows 1 crack which is almost horizontal, with less distress in the middle of the image. This is shown up as 2 peaks in the Hough transform domain, displaced by 52 pixels which is approximately 0.16 m, but having nearly the same orientation, indicating that they actually belong to the same crack. Crack length measured seems less than the actual length because of the many gaps that separate the crack. Cracks classification and measurements results are shown in Table 3.

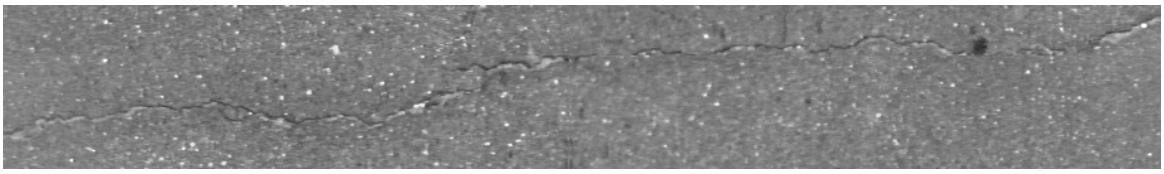

Figure 8-a. Original Image Sec. 273016026

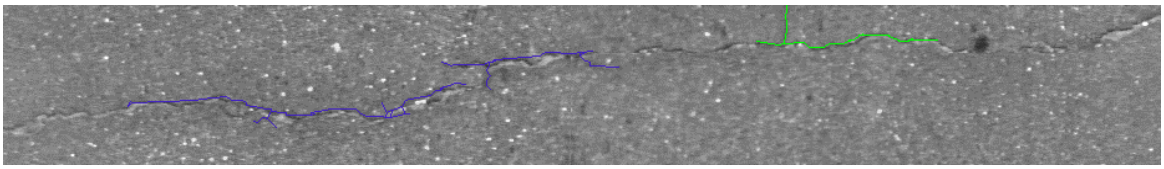

Figure 8-b. Cracks detected by Wisecrax®

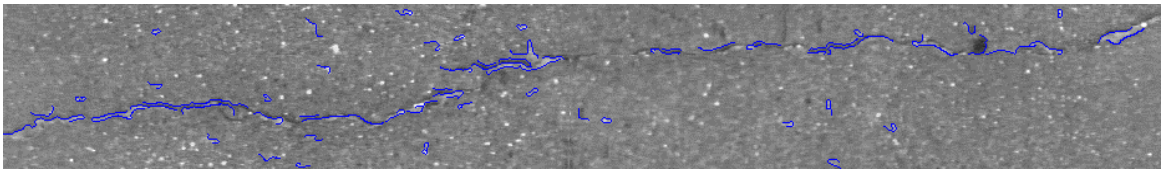

Figure 8-c. Cracks detected by multi-scale edge detection techniques.

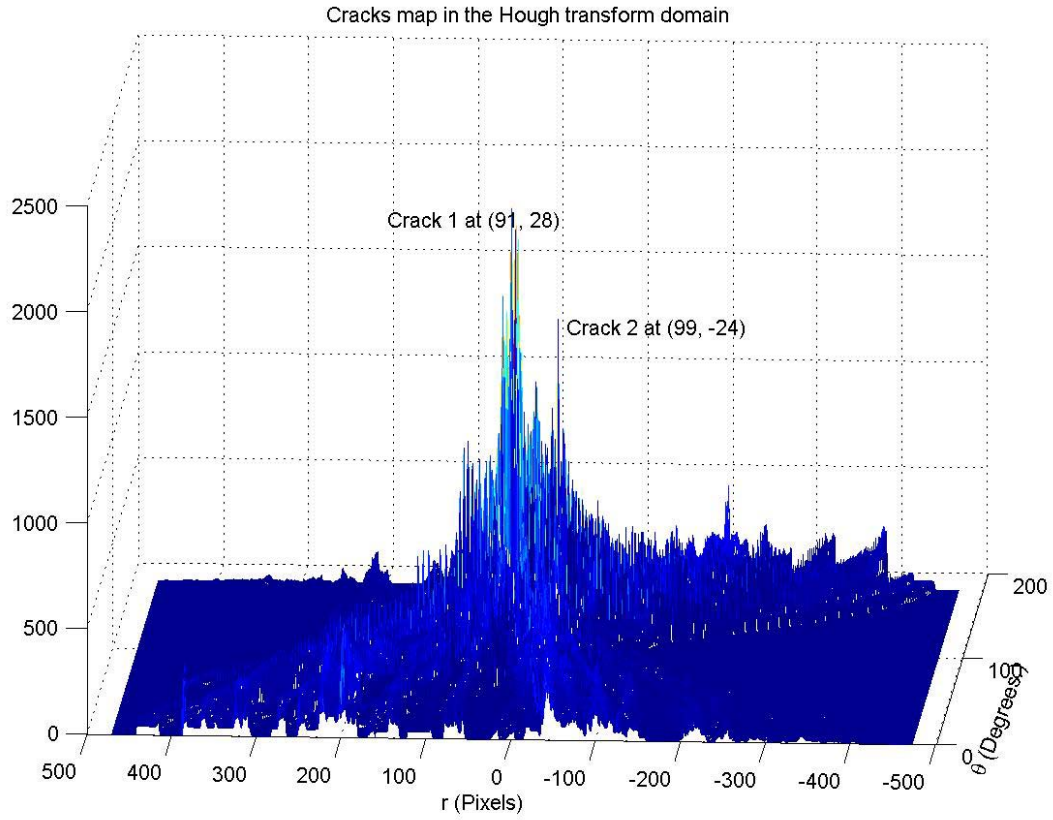

Figure 8-d. Cracks in the Hough transform domain. 1 crack is detected. θ measured from vertical in the original image.

Crack Number	Crack Length (m)	Crack Average Width (Pixels)	Crack Average Width (mm.)	Severity
1	1.9	5	16.2	High

Table 3. Results for Section 273016026

Section 273016013:

Figure 9-a shows a 260*200 pixels image, which is 0.9*0.7 meters^2 on the road. It shows 1 wide, almost horizontal crack, and 2 other smaller cracks, probably belong to the same crack; since their peaks are merged together in the Hough transform plane. Crack 1 is shorter, which is manifested by its lower peak. Crack width measurements are accurate; it reveals the difference in width for the three cracks. Crack 1 is so wide (about 3 cm.), crack 3 is classified as a medium severity crack. Cracks classification and measurements results are shown in Table 4.

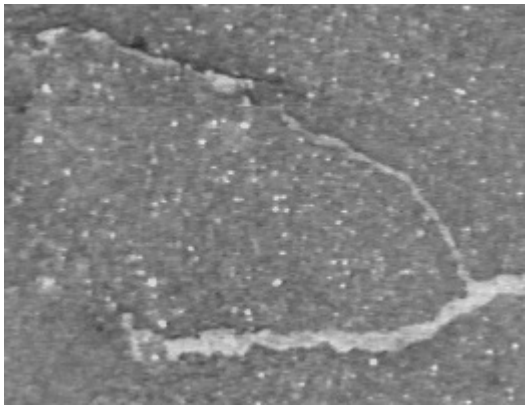

Figure 9-a. Original Image Sec. 273016013

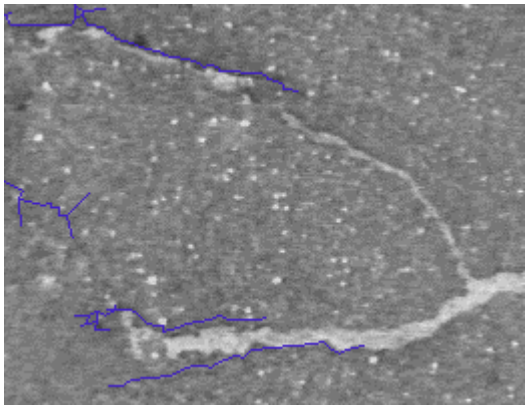

Figure 9-b. Cracks detected by Wisecrax®

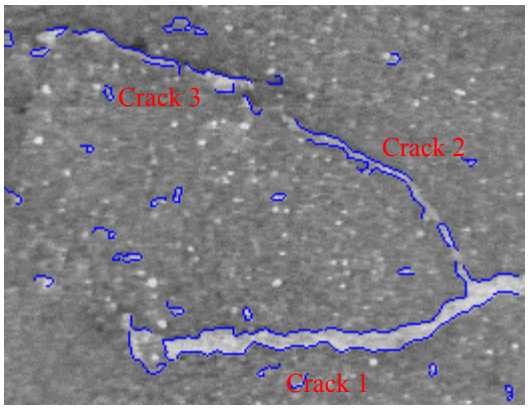

Figure 9-c. Cracks detected by multi-scale edge detection techniques.

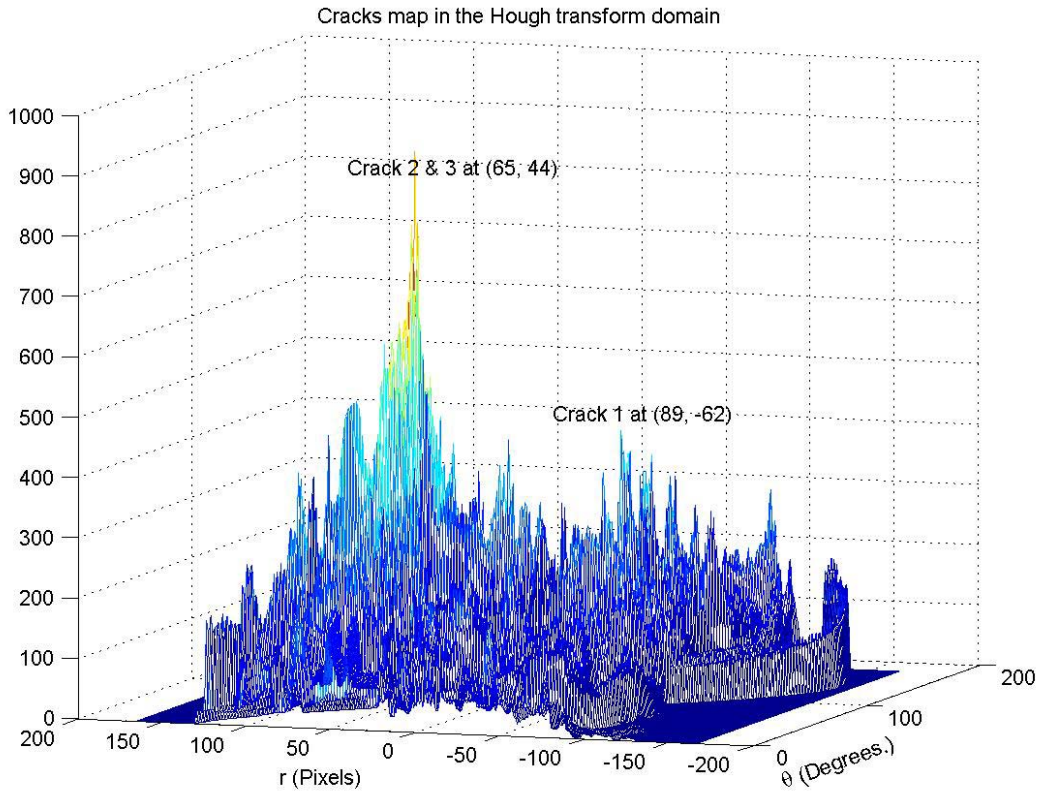

Figure 9-d. Cracks in the Hough transform domain. 3 cracks are detected. θ measured from vertical in the original image.

Crack Number	Crack Length (m)	Crack Average Width (Pixels)	Crack Average Width (mm.)	Severity
1	0.76	9.4	30.3	High
2	0.29	4.3	14	High
3	0.26	3.4	11.3	Medium

Table 4. Results for Section 273016013

Section 27301600118:

Figure 10-a shows a 530*100 pixels image, which is 1.8*0.33 meters^2 on the road. Detection shows 3 peaks, at $(89^\circ, 7), (88^\circ, 12), (92^\circ, -5)$. Clearly, they are almost overlapping, which may classify it as an alligator type of a crack. Cracks classification and measurements results are shown in Table 5.

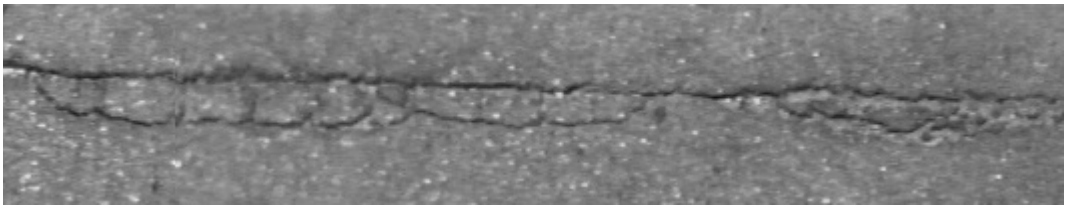

Figure 10-a. Original Image Sec. 27301600118

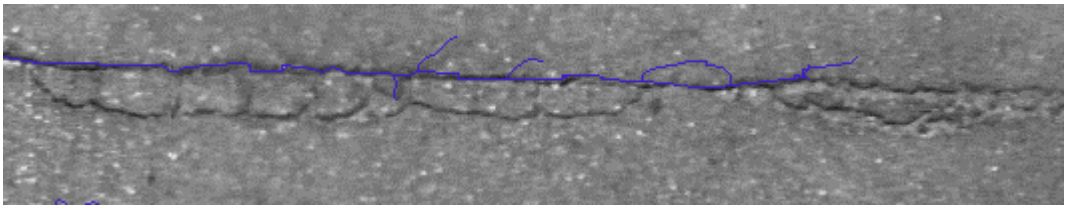

Figure 10-b. Cracks detected by Wisecrax®

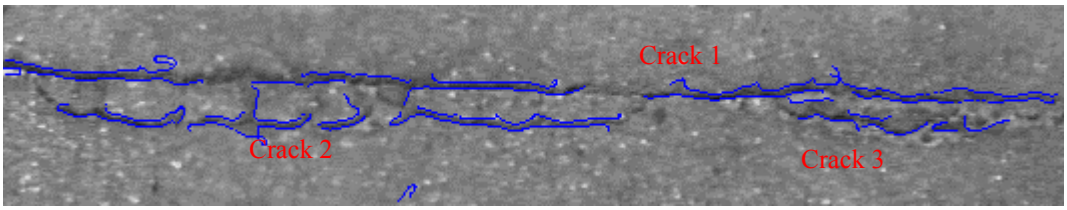

Figure 10-c. Cracks detected by multi-scale edge detection techniques.

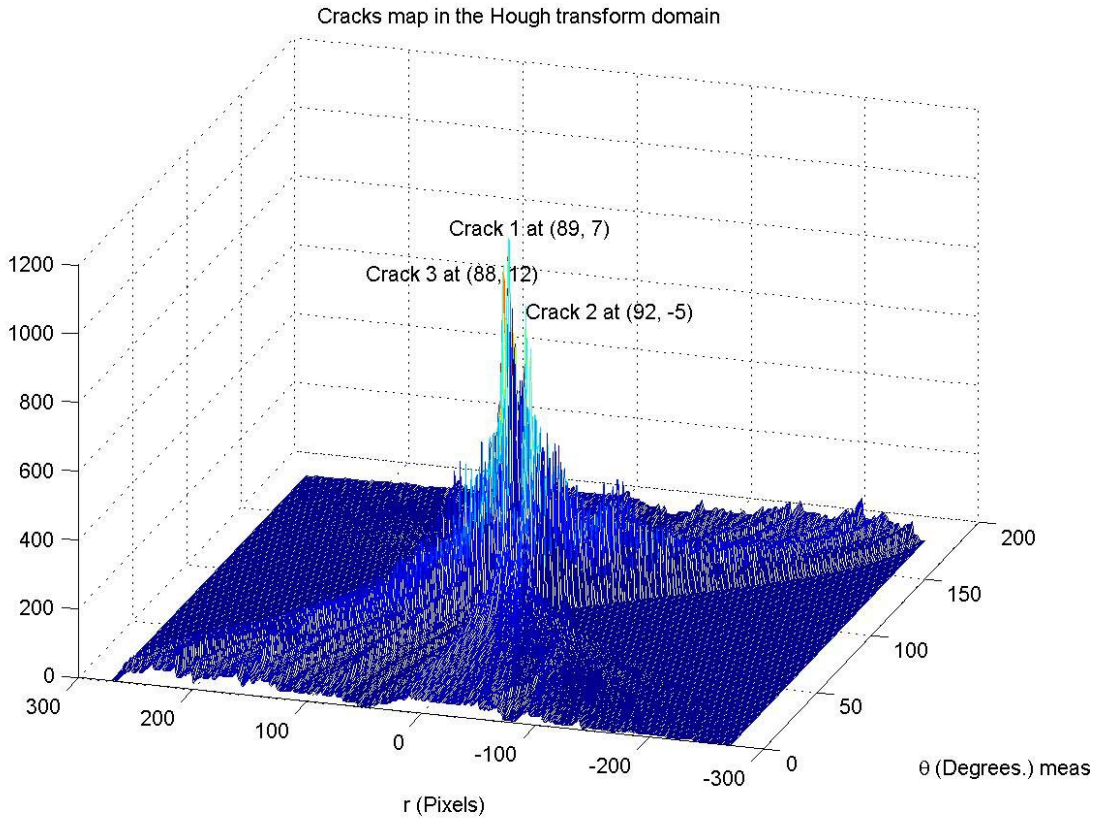

Figure 10-d. Cracks in the Hough transform domain. 3 cracks are detected. θ measured from vertical in the original image.

Crack Number	Crack Length (m)	Crack Average Width (Pixels)	Crack Average Width (mm.)	Severity
1	1.13	4	12.9	High
2	0.87	3.2	10.3	Medium
3	0.56	3.2	10.3	Medium

Table 5. Results for section 27301600118

Section 273016190:

Figure 11-a shows a 300*250 pixels image, which is 1*0.8 meters^2 on the road. This image is highly compressed, you can tell from the artifacts around the 8*8 uncorrelated blocks which can be clearly seen in figure 11-b. This problem is discussed in detail in section 7, and it is the reason for the many small false cracks detected all over the image. Three main cracks can be inferred from figure 11-e., oriented in three different directions $94^\circ, 130^\circ, 50^\circ$. Crack 3 has a lower peak; since it is shorter than cracks 1 and 2. The cracks are not very well defined, this is because of the resolution lost due to compression. This image is a good example of the

drawbacks of compression on the detection accuracy. Cracks classification and measurements results are shown in Table 6.

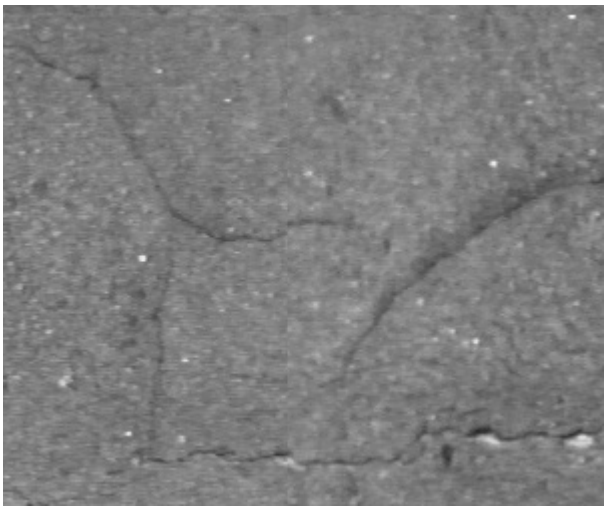

Figure 11-a. Original Image Sec. 273016190

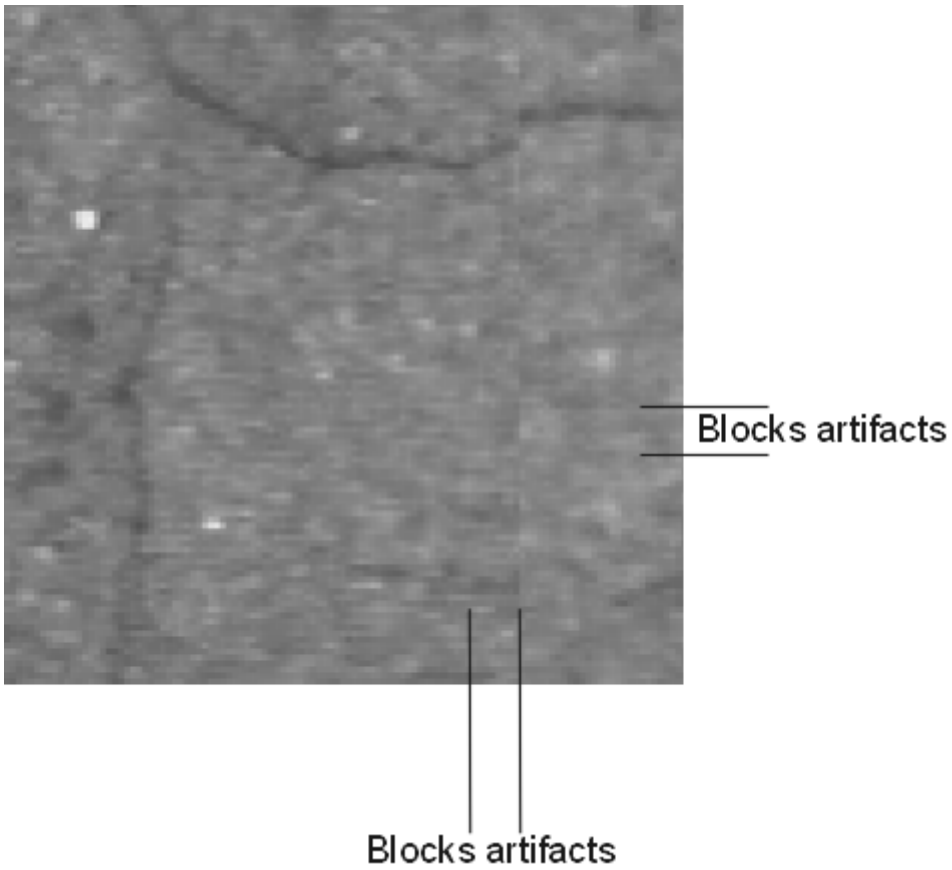

Figure 11-b. Distortions caused by high compression of the road images.

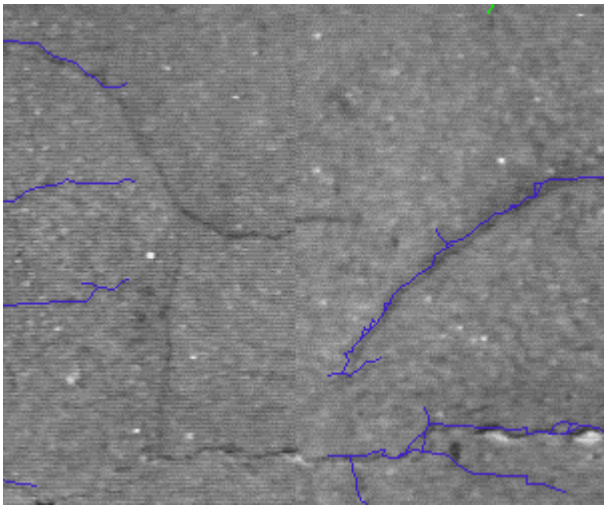

Figure 11-c. Cracks detected by Wisecrax®

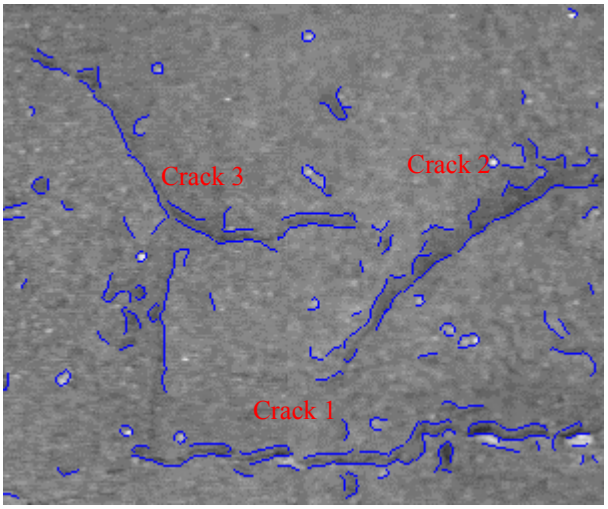

Figure 11-d. Cracks detected by multi-scale edge detection techniques.

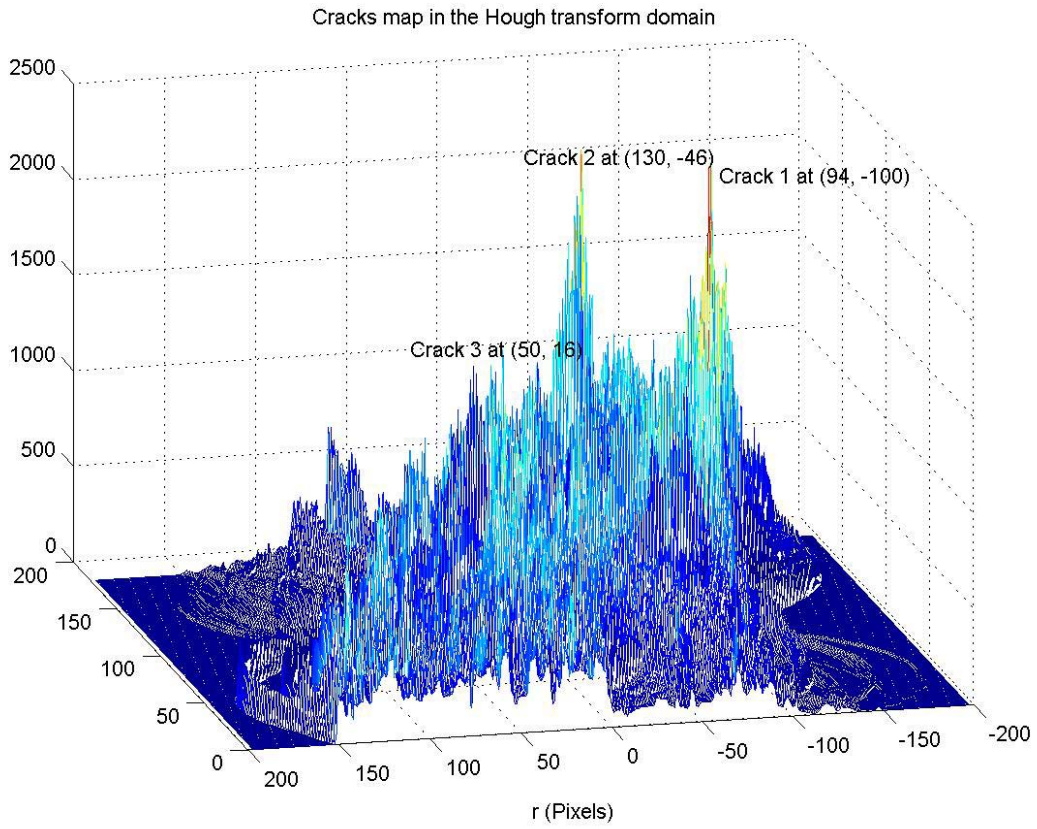

Figure 11-e. Cracks in the Hough transform domain. 3 cracks are detected. θ measured from vertical in the original image.

Crack Number	Crack Length (m)	Crack Average Width (Pixels)	Crack Average Width (mm.)	Severity
1	0.78	9.7	31.3	High
2	0.52	10.5	33.8	High
3	0.46	7.1	23.6	High

Table 6. Results for section 273016190

Section 273016092:

Figure 1-a shows a 580*150 pixels image, which is 1.9*0.5 meters^2 on the road. There are mainly 2 cracks. Crack 1 is transverse, and is well detected. It shows up as a peak at $(92^\circ, -8)$. Crack 2 is almost longitudinal at $(13^\circ, 215)$ and can be neglected; since it is short, and less than 30 cm. Cracks classification and measurements results are shown in Table 7.

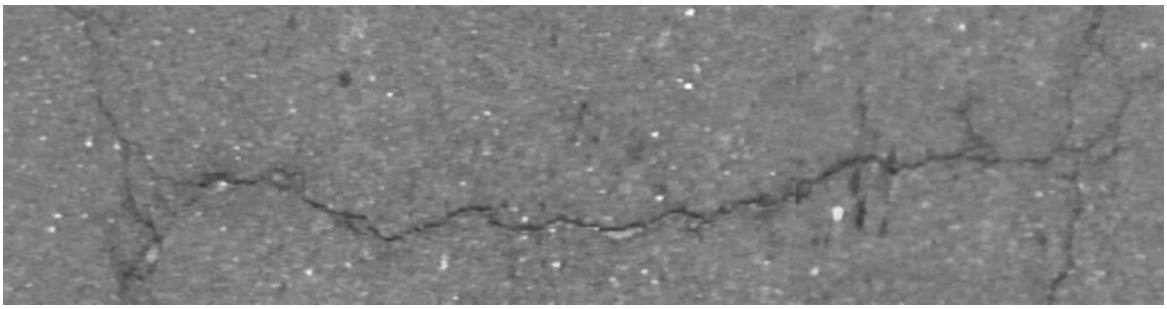

Figure 12-a. Original Image Sec. 273016092

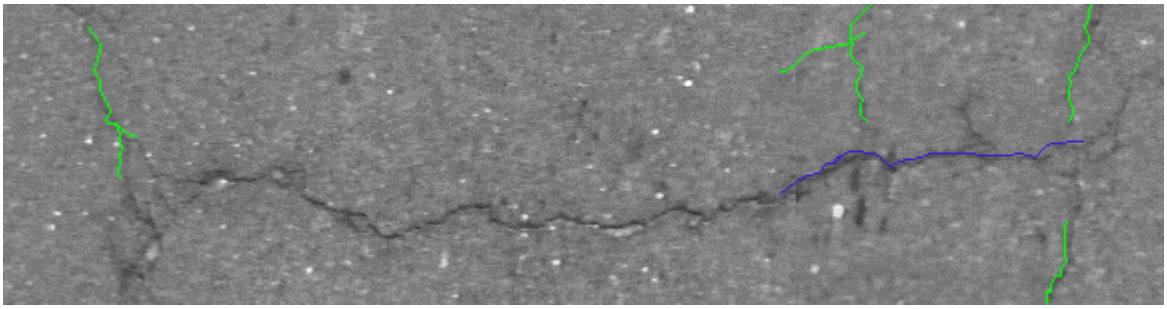

Figure 12-b. Cracks detected by Wisecrax®

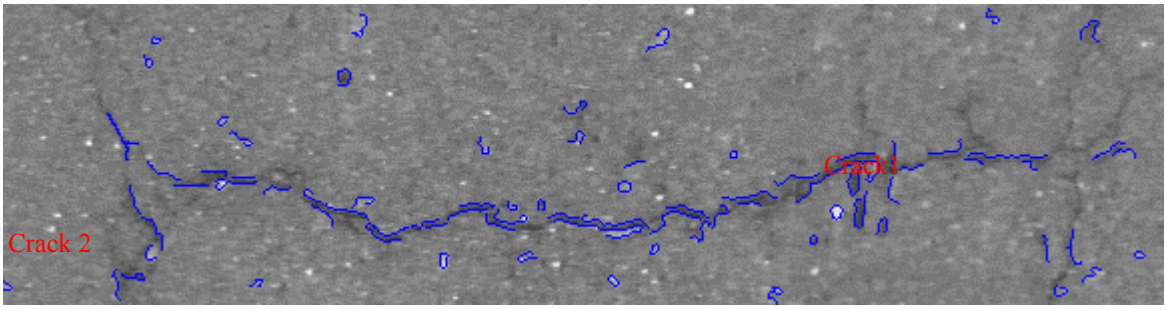

Figure 12-c. Cracks detected by multi-scale edge detection techniques.

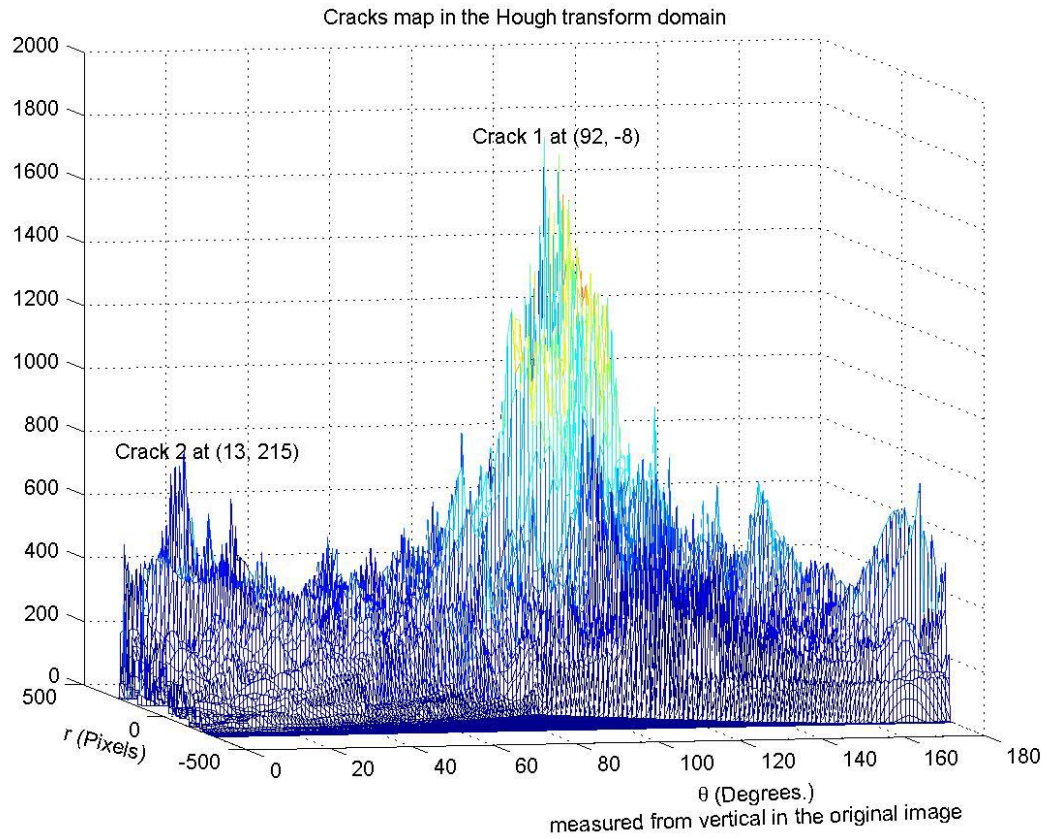

Figure 12-d. Cracks in the Hough transform domain. 3 cracks are detected. θ measured from vertical in the original image.

Crack Number	Crack Length (m)	Crack Average Width (Pixels)	Crack Average Width (mm.)	Severity
1	2.8	6.7	21.6	High
2	0.14	6.6	21.3	High

Table 7. Results for section 273016092

12. Future research planning

Based on the information gathered, a number of supplementary problems were identified with the Wisecrax® system but seen to be outside the scope of this project. Two project pre-proposals based on these ideas have been submitted to the Connecticut Cooperative Highway Research Program (CCHRP) 2003-2004.

The algorithms developed needs to be tested with more high-resolution images. We must have access to Wisecrax® videotaped records to extract uncompressed images. Various iterations back and forth between wavelet decomposition and the Hough transform on smaller sections of the images are anticipated to reveal better results

References

[1] Stephan Mallat and Sifen Zhong, "Characterization of signals from multiscale edges," *IEEE Transactions on Pattern Analysis and Machine Intelligence*, Vol. 14, No. 7, p. 710-732, July 1992.

[2] Gilbert Strang and Truong Nguyen, *Wavelets and Filter Banks*, Wellesley-Cambridge Press, 1997.

[3] J. Canny, "A computational approach to edge detection," *IEEE Trans. Putt. Anal. Machine Intell*igence, Vol. PAMI-8, pp. 679-698, 1986.

[4] Anil Jain, *Fundamentals of Digital Image Processing*, Englewood Cliffs, NJ: Prentice Hall Press, 1989.

[5] John Proakis and Dimitris Manolakis, *Digital Signal Processing*, NJ: Prentice Hall Press, 1996.

[6] Rafael Gonzalez and Richard Woods, *Digital Image Processing*, Addison-Wesley Co., 2002.

[7] Alan Willsky, W. Karl, P. Fieguth, M. Schneider, "Multiscale methods for the segmentation and reconstruction of signals and images," *IEEE Transactions on Image Processing*, Vol. 9, No. 3, March 2000.

[8] S. Mallat and W. L. Hwang, "Singularity detection and processing with wavelets," *IEEE Trans. Inform. Theory*, Vol. 38, No. 2, Mar. 1992.

[9] Phillipe Delagnes and Dominique Barba, "A Markov random field for rectilinear structure extraction in pavement distress image analysis," *Proceedings of the 1995 International Conference on Image Processing* (ICIP '95).

[10] Takayuki Nakata, Yue Bao, Naofumi Fujiwara, "Detection of position and orientation of an object using 3D Hough transform," *IEEE International Conference on Intelligent Vehicles*, 1998.

[11] Yves Delignon, A. Marzouki, and W. Pieczynski, "Estimation of generalized mixtures and its application in image segmentation," *IEEE Transactions on Image Processing*, Vol. 6, No. 10, October 1997.